

Estimates of the Wavenumber-Frequency Spectra for the Nonhomogeneous Streamwise Transition Flow Pressure Field

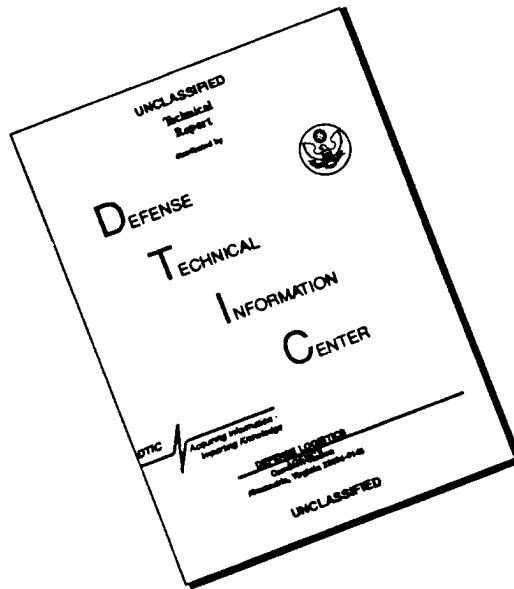
Ronald I. Ochsenknecht
Submarine Sonar Department



19960705 118

Naval Undersea Warfare Center Division
Newport, Rhode Island

DISCLAIMER NOTICE



THIS DOCUMENT IS BEST QUALITY AVAILABLE. THE COPY FURNISHED TO DTIC CONTAINED A SIGNIFICANT NUMBER OF PAGES WHICH DO NOT REPRODUCE LEGIBLY.

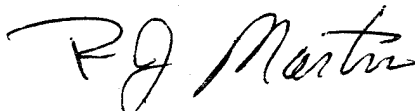
PREFACE

This report was prepared as a thesis for the degree of Master of Science in Acoustics awarded by Pennsylvania State University. The advisor for this research was Professor G. Lauchle.

The technical reviewer for this report was M. J. Berliner (Code 2141).

The author gratefully acknowledges Dr. Berliner for her careful review of the manuscript.

Reviewed and Approved: 14 June 1996

A handwritten signature in black ink, appearing to read "R J Martin". The signature is fluid and cursive, with the first letters of the first and last names being capitalized and prominent.

R. J. Martin
Acting Head, Submarine Sonar Department

TABLE OF CONTENTS

LIST OF FIGURES	v
LIST OF TABLES	vii
CHAPTER 1:INTRODUCTION	1
Background	1
Goals and Scope of Work	2
CHAPTER 2:SPACE-VARYING WAVENUMBER-FREQUENCY SPECTRUM	
OF TRANSITION FLOW PRESSURE FIELD	4
Space-Time Indicator Correlation Function	5
Finite Fourier Transform for Computer Estimation of Transition Flow	
Wavenumber Spectrum	8
Examples of Estimated Space-varying Transition Flow Wall Pressure	
Wavenumber Spectra	14
Summary of the Space-varying Wavenumber Spectra.	19
CHAPTER 3:TWO-WAVENUMBER-FREQUENCY SPECTRUM OF	
TRANSITION FLOW PRESSURE FIELD	20
Example Two-wavenumber Spectrum	20
Two-Wavenumber Transitional Flow Pressure Field Spectrum	30
Summary of the Two-Wavenumber Spectra.	35
CHAPTER 4:CONCLUSIONS AND RECOMMENDATIONS	36
REFERENCES	38

LIST OF FIGURES

v

Figure 1. Contour Plot of Space-Time Correlation of Intermittency	6
Figure 2. Contour Plot of Space-Time Correlation of Intermittency	7
Figure 3. Contour Plot of Space-Time Correlation of Intermittency	8
Figure 4. Probe location array	11
Figure 5. Estimated Space-Varying Streamwise Wavenumber Spectrum	15
Figure 6. Estimated Space-Varying Streamwise Wavenumber Spectrum	16
Figure 7. Estimated Space-Varying Streamwise Wavenumber Spectrum	18
Figure 8. Spatial Decay Characteristics of Example Harmonic Wave	21
Figure 9. Surface Plot of Exponentially Decaying Single Harmonic Wave True Two-Wavenumber Spectrum	23
Figure 10. Contour Plot of Exponentially Decaying Single Harmonic Wave Two Wavenumber Spectrum	24
Figure 11. Contour Plot of Two-Wavenumber Spectrum for Unidirectional Exponentially Damped Wave (From Kennedy and Strawderman)	25
Figure 12. Surface Plot of Estimated Two-Wavenumber Spectrum of Example Exponentially Decaying Single Harmonic Wave Using Unit Spatial Weighting	26
Figure 13. Contour Plot of Estimated Two-Wavenumber Spectrum of Example Exponentially Decaying Single Harmonic Wave Using Unit Spatial Weighting	27
Figure 14. Surface Plot of Estimated Two-Wavenumber Spectrum of Example Exponentially Decaying Single Harmonic Wave Using Taylor Spatial Weighting	28

List of Figures (continued)

Figure 15. Contour Plot of Estimated Two-Wavenumber Spectrum of Example Exponentially Decaying Single Harmonic Wave Using Taylor Spatial Weighting	29
Figure 16. Surface Plot of Estimated Streamwise Transitional Flow Pressure Field Two-Wavenumber Spectrum at 50 Hz	31
Figure 17. Contour Plot of Estimated Streamwise Transition Flow Pressure Field Two-Wavenumber Spectrum at 50 Hz.....	32
Figure 18. Surface Plot of Estimated Streamwise Transition Flow Pressure Field Two-Wavenumber Spectrum at 100 Hz.....	33
Figure 19. Contour Plot of Estimated Streamwise Transition Flow Pressure Field Two-Wavenumber Spectrum at 100 Hz.....	34

LIST OF TABLES

Table 1. Parameters of the Measured Transition Zones.....	13
---	----

CHAPTER 1

INTRODUCTION

Background

Continued research of the subsonic boundary layer laminar-to-turbulent transition zone wall pressure fluctuations has resulted in the formulation of an empirical space-time correlation model of the pressure field. Josserand and Lauchle¹ developed the empirical model, by determining the parameters of assumed functional forms, from extensive measurements of spot formation in the transition zone. They measured a "zero-one" function, an indicator function, that identifies the presence of turbulent spots. The space-time correlation model of the indicator function provides the fundamental statistics of the stationary, non-homogenous pressure field. However, the preferred format of this pressure field, for descriptive and interpretation purposes, is the wavevector-frequency spectrum. The wavevector-frequency spectrum is obtained by Fourier transformation of the space-time correlation. Two complications arise when attempting the Fourier transformation. First, the relatively complex form of this empirically derived correlation function defies the analytical integration required to produce the desired wavevector-frequency spectrum. Second, since the pressure field is non-homogeneous, the resulting

wavevector-frequency spectrum will be a function of reference position. This dependence on reference position precludes a concise description of the field. That is, for a homogeneous pressure field, a single wavevector-frequency spectrum describes the field. For a non-homogeneous pressure field no single wavevector-frequency spectrum describes the field. In fact, an infinity of spectra are required. Therefore, although the wavevector-frequency spectrum is the preferred format, a more concise spectral description is desired. Strawderman² has recently identified a full spectral definition of a non-homogeneous field. This thesis will investigate the application of both spectral forms to the study of boundary layer transitional flow pressure fluctuations.

Goals and Scope of Work

The objective of this research is to extend the work of Josserand and Lauchle by computing two forms of the wavevector-frequency spectrum of transition flow. First, the space-varying wavevector-frequency spectrum will be estimated using computer implemented numerical methods. Second, in an attempt to provide a more concise wavevector-frequency description of this non-homogeneous field, a recently developed spectral format named the "Two - Wavevector - Frequency "²spectrum will be computed. These computations will require multi-dimensional Fourier transformation of the empirically derived space-time correlation function of the boundary layer indicator function. The extent of the fundamental dimensionality of these transformations is great. In general, one temporal and two independent spatial vectors are required. Techniques to image these dimensions are not generally available and are beyond the scope of the

present investigation. Therefore it is necessary to select a useful but reduced domain of interest.

It is known that the major features of turbulent flow are contained in the streamwise component. Investigation of the characteristics of the space-time correlation of transitional flow reveal similar major features. Therefore it is considered appropriate to limit the dimensionality of the current investigation to the streamwise component of transition flow.

This will require satisfying the following goals;

1. Implement a computer model of the indicator function space-time correlation function.
2. Compute the Fourier transform of the indicator function space-time correlation function on streamwise wavenumber and frequency, at selected reference positions in the transition zone, to estimate the space varying wavenumber-frequency spectrum of transitional flow.
3. Compute the Fourier transform of the indicator function space-time correlation function on streamwise wavenumber, frequency, and reference position to estimate the two wavenumber-frequency spectrum of transitional flow.

CHAPTER 2

SPACE-VARYING WAVENUMBER-FREQUENCY SPECTRUM OF TRANSITION FLOW PRESSURE FIELD

The wavenumber-frequency spectrum of boundary layer transitional flow wall pressure fluctuations is defined¹ as

$$\Phi_{trans}(\eta_1, k_1, k_3, \omega) = \frac{1}{(2\pi)^3} \int_{-\infty}^{+\infty} \int_{-\infty}^{+\infty} \int_{-\infty}^{+\infty} R_l(\eta_1, \varepsilon_1, \varepsilon_3, \tau) \times R_{turb}(\varepsilon_1, \varepsilon_3, \tau) e^{-i(k_1 \varepsilon_1 + k_3 \varepsilon_3 - \omega \tau)} d\varepsilon_1 d\varepsilon_3 d\tau \quad (1)$$

Here η_1 denotes absolute position within the transition zone, ε_1 is longitudinal spatial lag, relative to η_1 , and ε_3 is transverse spatial lag. Temporal lag is denoted by τ . Longitudinal and transverse wavenumber are denoted by k_1 and k_3 , ω is radian temporal frequency.

The function $R_l(\eta_1, \varepsilon_1, \varepsilon_3, \tau)$ is the space-time correlation of the indicator process and $R_{turb}(\varepsilon_1, \varepsilon_3, \tau)$ is the space-time correlation of the turbulent flow wall pressure fluctuations, presumed homogeneous within the turbulent spots of the transition zone. The correlation function $R_l(\eta_1, \varepsilon_1, \varepsilon_3, \tau)$ is derived empirically from measurements of the statistics of transition zone spot formation and contains the non-homogeneous characteristics of interest here. The correlation $R_{turb}(\varepsilon_1, \varepsilon_3, \tau)$ is the homogeneous component and contains no information from the transition zone. Considering this, and recalling the previous discussion regarding the desire to reduce the dimensionality to

streamwise flow only ($\varepsilon_3 = 0$), it is appropriate to write the pertinent wavenumber-frequency spectrum as

$$\Psi_I(\eta_1, k_1, \omega) = \frac{1}{(2\pi)^2} \int_{-\infty}^{+\infty} \int_{-\infty}^{+\infty} R_I(\eta_1, \varepsilon_1, 0, \tau) e^{-i(k_1 \varepsilon_1 - \omega \tau)} d\varepsilon_1 d\tau \quad (2)$$

Space-Time Indicator Correlation Function

The space-time correlation of intermittency has been determined³ empirically to be

$$\begin{aligned} R(\eta_1, \varepsilon_1, \varepsilon_3, \tau) = & \gamma_u(\eta_1) \left[\gamma_d(\eta_1) + (1 - \gamma_d(\eta_1)) \exp \left\{ -5 \left(4 + 200 \left| \tau - \frac{\varepsilon_1}{U_c} \right| \right) \left| \tau - \frac{\varepsilon_1}{U_c} \right| \right\} \right. \\ & \exp \left(20 \frac{|\varepsilon_1|}{0.014 \Delta x + |\varepsilon_1|} \left| \tau - \frac{\varepsilon_1}{U_c} \right| \right) \\ & \exp \left(-4 - \frac{320 \left| \tau - \frac{\varepsilon_1}{U_c} \right|}{\Delta x + 71 |\varepsilon_3|} \frac{|\varepsilon_3| \Delta x}{0.254 + 3.6 |\varepsilon_1|} \right) \Big] \\ & \exp \left[- \frac{A |\Lambda_1|}{0.0014 + |\Lambda_1|} \frac{1}{1 + 1300 \left| \tau - \frac{\varepsilon_1}{U_c} \right|^2} \right] \end{aligned} \quad (3)$$

Here, γ_u is the intermittency measured by the upstream probe and γ_d is the intermittency measured by the downstream probe. The convection velocity is U_c , Δx

is the streamwise length of the transition zone, Λ_1 is the normalized longitudinal separation inside the transition zone, $\varepsilon_1/\Delta x$, and $A = -\ln[1 - \exp(-4.27/\Delta x)]$ with Δx in meters. In general, the intermittency is written as $\gamma(z) = 1 - \exp[-(1 - 3.4z)z^2]$ with $z = \eta_1/\Delta x$.

It is useful to identify the η_1 dependence of (3) for $\varepsilon_3 = 0$. This dependence is qualitatively demonstrated in the contour plots shown in Figures 1, 2, and 3. These contour plots were generated for $\Delta x = 1.04$ m and three arbitrarily selected values of η_1 : 0.1040, 0.5200, and 0.8320 meter from which z ranges from 0.1 to 0.8. Note that each of the figures can be described in terms of only two processes that occur to

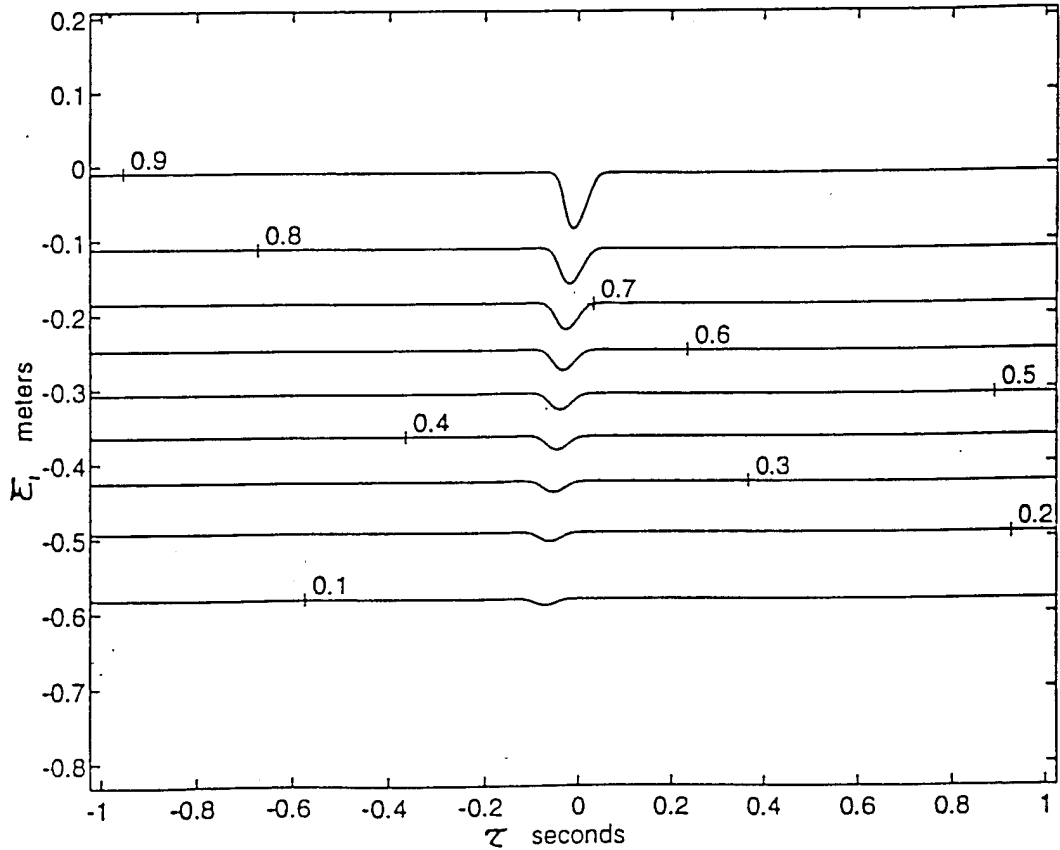


Figure 1. Contour Plot of Space-Time Correlation of Intermittency; $z = 0.8$

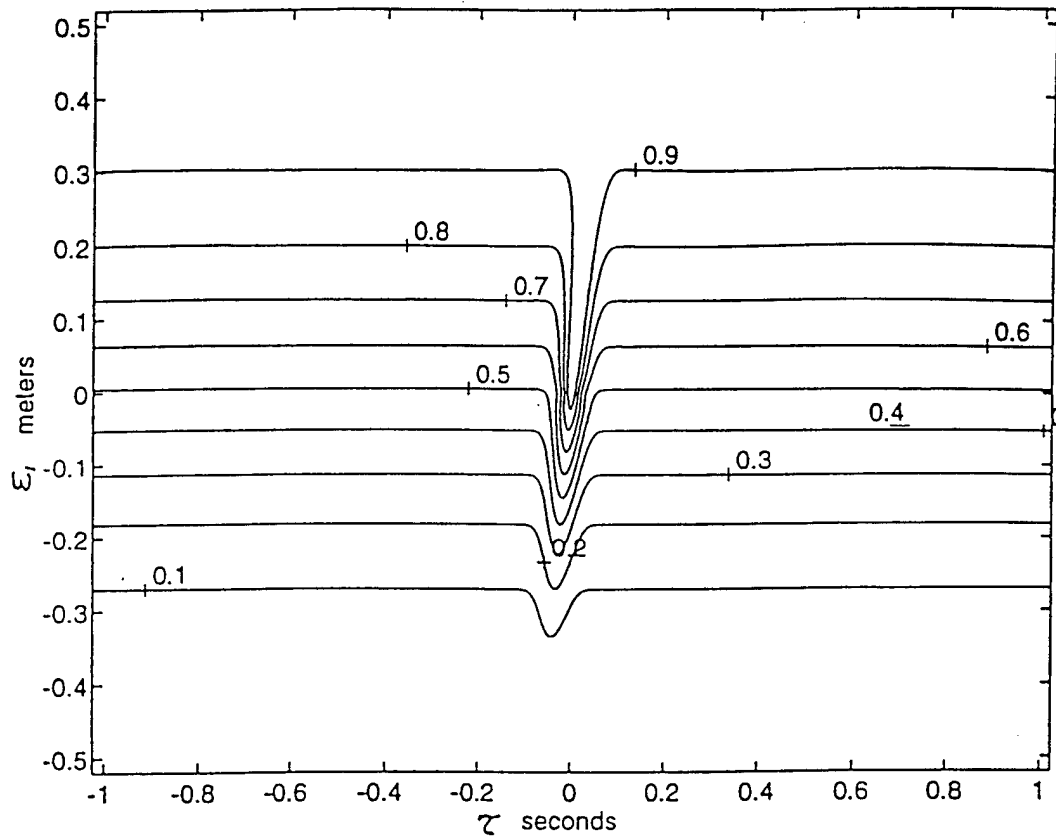


Figure 2. Contour Plot of Space-Time Correlation of Intermittency; $z = 0.5$

varying degrees as a function of reference location (η_1). One process has correlation that varies only with spatial lag. The other process is highly correlated over only a small temporal region. The time lag, associated with the peak in correlation, varies with spatial separation indicating propagation. This propagating component has a velocity of approximately 8.23 m/sec, and is consistent with the selected convection velocity.

In summary, these figures demonstrate the expected convective component of intermittent turbulent flow, as well as the position dependent (non-homogeneous) nature of the transition flow pressure field, in terms of space-time correlation.

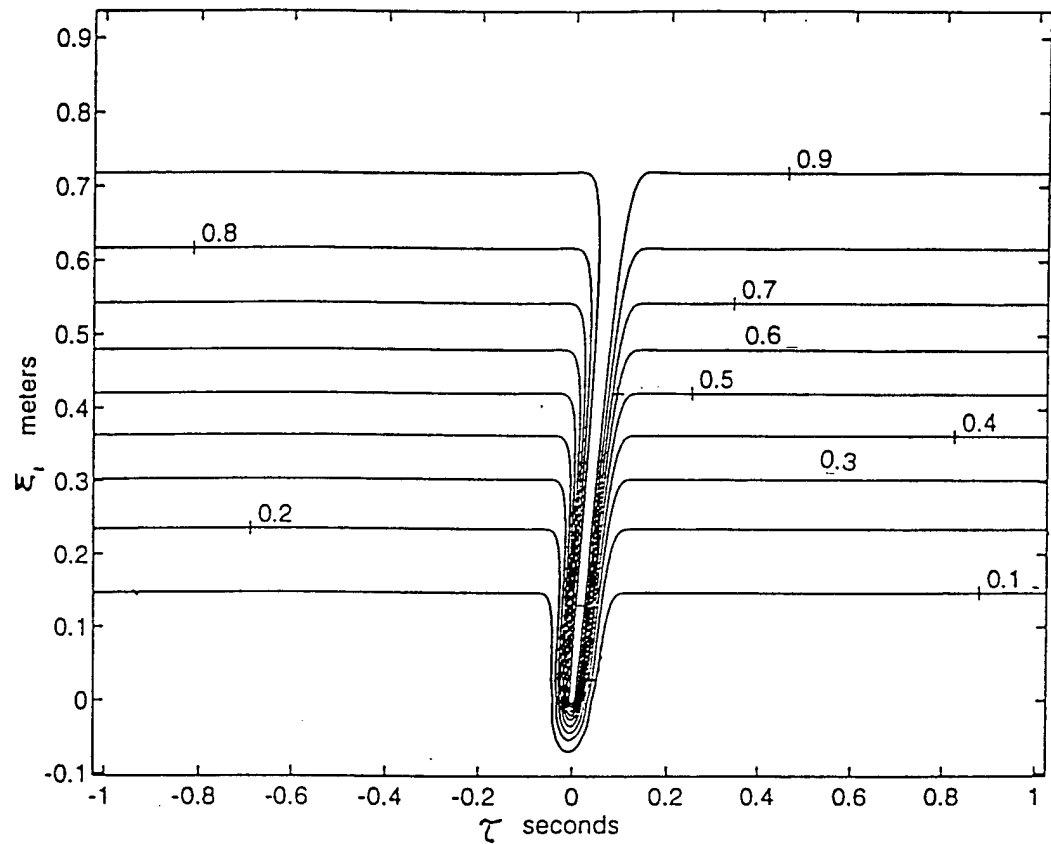


Figure 3. Contour Plot of Space-Time Correlation of Intermittency; $z = 0.1$

Finite Fourier Transform for Computer Estimation of Transition Flow Wavenumber Spectrum

The pertinent wavenumber spectrum of transition flow is defined by (2). However, as previously stated, a digital computer will be used to generate numerical spectral estimates. The computer implementation requires a finite, discrete, form of (2). The consequence of the required, finite length, space-time sampling, is spectral amplitude

bias, where spectral amplitude bias is defined ⁴ as the difference between the spectral estimate and the true spectrum.

The concept of spectral bias can be developed from the realization that finite, discrete space-time correlation sample sets are obtained from continuous, infinite space-time correlation functions, by multiplication by appropriate sampling functions. The wavenumber-frequency spectrum is therefore the Fourier transform of a product. The Fourier transform of a product is equivalent to the convolution of the Fourier transforms of the individual functions. Therefore, the streamwise wavenumber-frequency spectrum may be thought of as the convolution of the two dimensional Fourier transform of the space-time sampling function with the true wavenumber-frequency spectrum. The Fourier transform of a finite length space-time sampling function will contain a main response lobe of finite width. Therefore, a spectral estimate at any given wavenumber and frequency, comprises an integral of the true wavenumber-frequency spectrum giving rise to spectral amplitude bias.

Spectral bias is the combined effect of: 1) aliasing⁵ resulting from sampling at uniform intervals, 2) decreased spectral resolution⁶ resulting from finite length sample sets, 3) sidelobe leakage⁷ caused by discontinuities at the sample set boundary. Windowing techniques exist, and will be used in this research, to mitigate the effects of sidelobe leakage. Spectral aliasing is an inherent consequence of sampling. However, aliasing occurs in a systematic manner allowing meaningful data interpretations to be made for some relatively uncomplicated cases.

Decreased spectral resolution is particularly troublesome. The spectral amplitude bias caused by decreased spectral resolution can be reduced or eliminated by appropriate scaling terms if the resolution and bandwidth of the process of interest are known apriori. The resolution can be determined from knowledge of the space-time sampling parameters. In as much as a goal of this research is to provide unprecedented

images of two transitional flow pressure field spectral formats, it follows that the process bandwidth is a desired result, and therefore, not known apriori. Consequently, any computer implemented spectral calculation is subject to spectral amplitude bias and thus can only estimate the true spectrum⁸. It should be emphasized that the impact of spectral bias is to introduce an unknown amplitude scaling term. Spectral shape characteristics, which provide the fundamental basis for interpretation, are not affected. Therefore, the impact of spectral bias on this research is minimal. Considering these factors it is deemed appropriate to write the required finite, discrete form of (2) as

$$\begin{aligned} \hat{\Psi}_I(\eta_1, k_1, \omega) \propto & \sum_{n=1}^N \sum_{m=1}^M w_{\varepsilon_1}(n\Delta\varepsilon_1) w_{\tau}(m\Delta\tau) R_I(\eta_1, n\Delta\varepsilon_1, m\Delta\tau) \\ & \times e^{-i(k_1 n\Delta\varepsilon_1 - \omega m\Delta\tau)} \Delta\varepsilon_1 \Delta\tau \end{aligned} \quad (4)$$

where the proportionality is used to reflect the amplitude uncertainty.

This implementation requires selection of finite sets of discrete values for the transform variables n , m , $\Delta\varepsilon_1$ and $\Delta\tau$ as well as spatial and temporal weighting functions $w_{\varepsilon_1}(n\Delta\varepsilon_1)$, and $w_{\tau}(m\Delta\tau)$. Since $R_I(\eta_1, \varepsilon_1, \varepsilon_3, \tau)$ was empirically derived it is considered appropriate to select the required computer model sampling parameters consistent with those of the measurement apparatus. Pertinent parameters of that measurement apparatus are discussed in the following section.

The space-time correlation of transition flow pressure was obtained by indirect methods. Measurements of boundary layer spot formation in the transition zone were obtained from an array of hot film sensors⁹ as shown in Figure 4. The actual measurement process consisted of sequential data acquisitions from discrete sensor pairs.

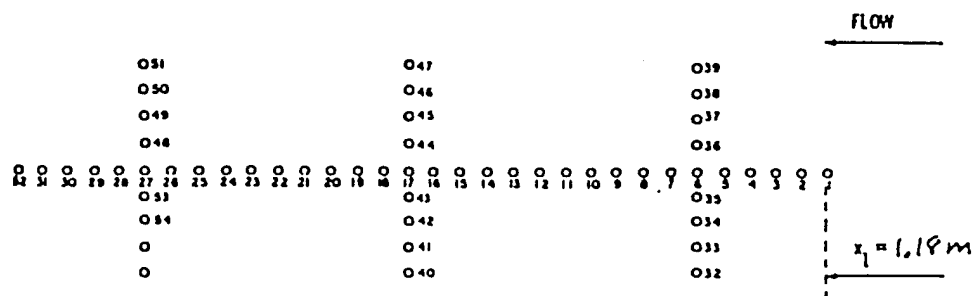


Figure 4. Probe location array

This data set was used to generate parameters for assumed functional forms of the indicator function space-time correlation. However, noting that the data were obtained from an "array" of spatially distributed sensors, it is useful to perceive of $R_I(\eta_1, \varepsilon_1, \varepsilon_3, \tau)$ having been obtained by direct measurement. That is, consider replacing the hot film sensors by pressure sensors. Acquiring data from all pressure sensors, simultaneously, would provide a direct measurement of the transition zone wall pressure fluctuations. Array signal processing techniques could then be applied to the discrete pressure measurements to produce the wavenumber spectrum of transition zone wall pressure. This concept of considering the hot film sensors to be a "virtual array" of pressure sensors is the basis for the selection of the sampling characteristics of the computer model. Because only the streamwise component is considered in this current research, the required transform parameters are the rate and quantity of temporal and spatial samples from the elements of a linear array.

The temporal sampling rate was selected to preclude temporal aliasing at frequencies of interest consistent with those in reference (1). This requires¹⁰ at least two samples of each period at the highest frequency of interest. Typically, frequencies of

100 Hz or less were considered requiring a Nyquist, or minimum, sampling frequency of 200 Hz. Sampling in excess of this minimum value is desired. Therefore, the temporal sampling rate was selected to be 250 Hz corresponding to a sample interval of 0.0040 seconds. Associated with this temporal sampling rate is the assumption that the measured data was low pass filtered to eliminate frequencies greater than 100 Hz. The number of temporal samples was selected to be 513.

Similar sampling criteria applies to the spatial domain. Here, the desire to simulate the measurement apparatus defines the spatial sampling rate. From Figure 4, the linear section consists of thirty two locations separated by 2.54 cm, thus dictating a 2.54 cm spatial sampling rate. Strawderman¹¹ identifies the consequence of this uniform spatial sampling rate as spatial aliasing of spectra at wavenumbers greater than $\pi/\Delta\epsilon_1$. This means that, for the 2.54 cm spatial sampling rate, components of the wavenumber spectrum in the range $|k_1| < 123.7$ rad/m will be located at their actual (unaliased) position. However, spectral components having higher wavenumbers will be aliased into the wavenumber range of $|k_1| < 123.7$ rad/m. The true wavenumber of unaliased spectral components can be estimated by realizing that the true wavenumber location is separated from the aliased wavenumber by an integer multiple of $2\pi/\Delta\epsilon_1$ ¹². Therefore, although the occurrence of spatial aliasing associated with implementing uniform spatial sampling confounds data interpretation, it does not preclude it.

The nominal length of the measurement array is approximately 0.81 m. However, from Table 1, the length of the transition zone was always somewhat greater than the array length (1.00 to 1.24 m). Therefore, in an attempt to simulate the spectral resolution of an aperture consistent with the nominal length of the transition zone, but not

deviate greatly from that of the actual measurement apparatus, the number of sensors was selected to be forty one.

Table 1. Parameters of the Measured Transition Zones¹.

Flow Velocity U_{∞} (m/s)	Measured Intermittency Range	Transition Length Δx (m)	Transition Point x_0 (m)
11.2	0.08 - 0.60	1.24	0.990
11.77	0.17 - 0.80	1.04	0.914
12.6	0.40 - 0.99	1.00	0.863

Implementation of the spatial and temporal sampling parameters implies multiplication of $R_l(\eta_1, \epsilon_1, \epsilon_3, \tau)$ by finite length, unit amplitude sampling functions. The Fourier transform of these finite length, unit amplitude, sampling functions are infinite length, periodic, spectral representations that comprise mainlobe and sidelobe structure. Unit amplitude weighting, applied to a given length sample set, produces the narrowest mainlobes and highest sidelobes. The narrow mainlobe is advantageous. However, the high sidelobes typically contribute unacceptable spectral estimation error via sidelobe leakage. This sidelobe leakage can be reduced by the use of window functions having other than unit amplitude coefficients. Many windows have been developed. In general, the consequence of other than unit amplitude windows is broader mainlobes and reduced sidelobes. Therefore, the decision regarding the need for a window involves a trade-off between spectral resolution and sidelobe leakage. Because this research involves the pressure field of a turbulent boundary layer, known to contain high energy levels concentrated at specific regions of the wavenumber domain, a window was deemed

necessary to reduce sidelobe leakage. A Taylor¹³ weighting function was selected, for both the spatial and temporal windows. This weighting function may be written as:

$$w(p) = \frac{1}{2\pi} \left\{ F(0) + 2 \sum_{m=1}^{\bar{n}-1} F(m) \cos(mp) \right\}, |p| \leq \pi \quad (5)$$

$$\text{where } F(m) = \prod_{n=1}^{\bar{n}-1} \left[1 - \frac{\frac{m^2}{\sigma^2 \left(A^2 + \left(n - \frac{1}{2} \right)^2 \right)} \sin(\pi m)}{1 - \frac{m^2}{n^2}} \right] \quad (6)$$

$$\text{and } \bar{n} = \text{number of "near-in" nulls, } \sigma = \bar{n} / \sqrt{A^2 + \left(\bar{n} - \frac{1}{2} \right)^2}, \quad (7)$$

$$A = \frac{1}{\pi} \ln \left(R + \sqrt{R^2 - 1} \right), \quad (8)$$

$R = 10^{\frac{|S|}{20}}$, and S = the maximum sidelobe level in dB.

Examples of Estimated Space-varying Transition Flow

Wall Pressure Wavenumber Spectra

The space-varying wavenumber spectrum was calculated for two frequencies at reference positions of $z = 0.1, 0.5$, and 0.8 . These reference positions are consistent with those chosen for the space-time correlation of intermittency. The computed spectra for 50 Hz are shown in Figure 5. Note that the abscissa is wavenumber, non-dimensionalized by transition zone length (1.04 m for this case). Interpretation of these spectra reveal that there are clearly two, and perhaps three, coherent processes visible above the underlying incoherent component. The most prominent is that occurring at

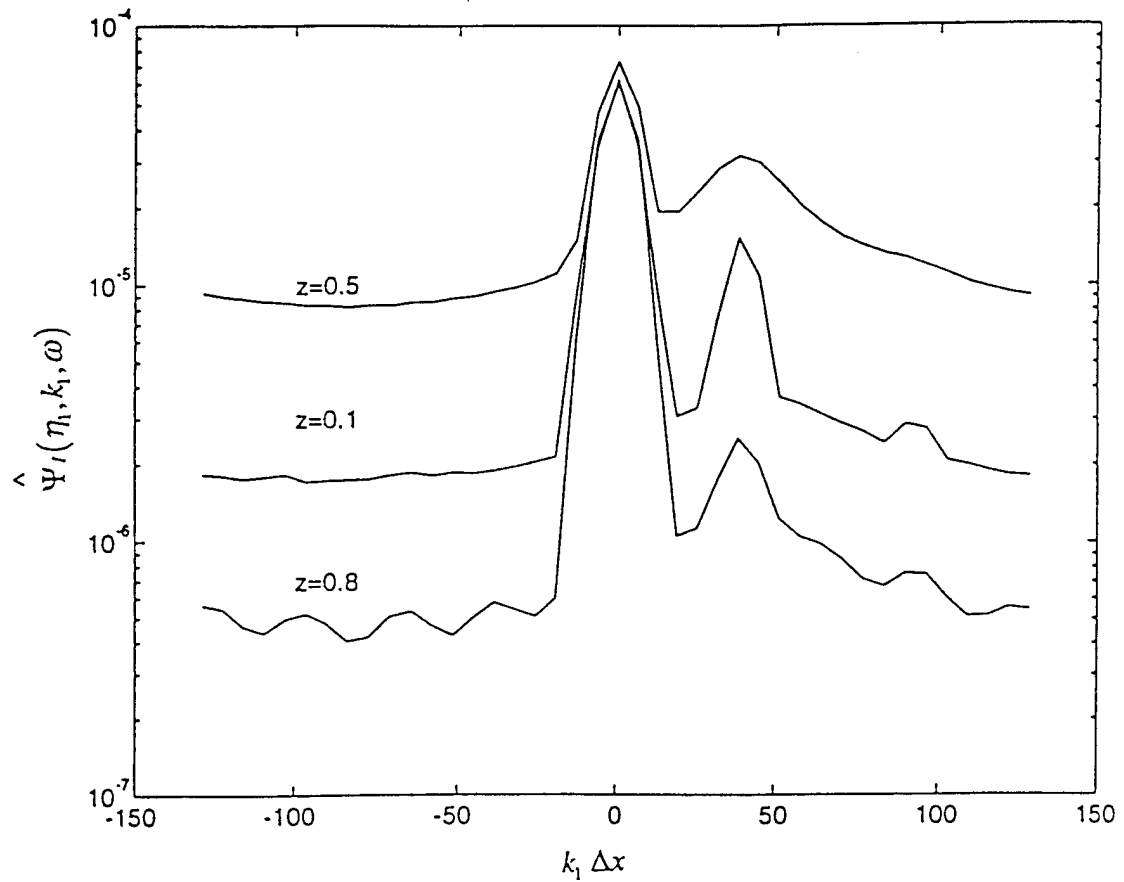


Figure 5. Estimated Space-Varying Streamwise Wavenumber Spectrum; 50 Hz

zero wavenumber. Energy in this region of the wavenumber spectrum can occur from at least two different processes. One possibility is that the spectra are of acoustic origin. Another is that they reflect the mean values of the random processes. The origin of this component was resolved by eliminating the mean value from the space-time correlation function and re-computing the space-varying wavenumber spectra. As shown in Figure 6, the prominent feature at $k_1=0$ has been eliminated. Clearly this component was the result of the mean value contained in the space-time correlation function. In as much as this research focuses on the dynamic characteristics of transition flow wall pressure,

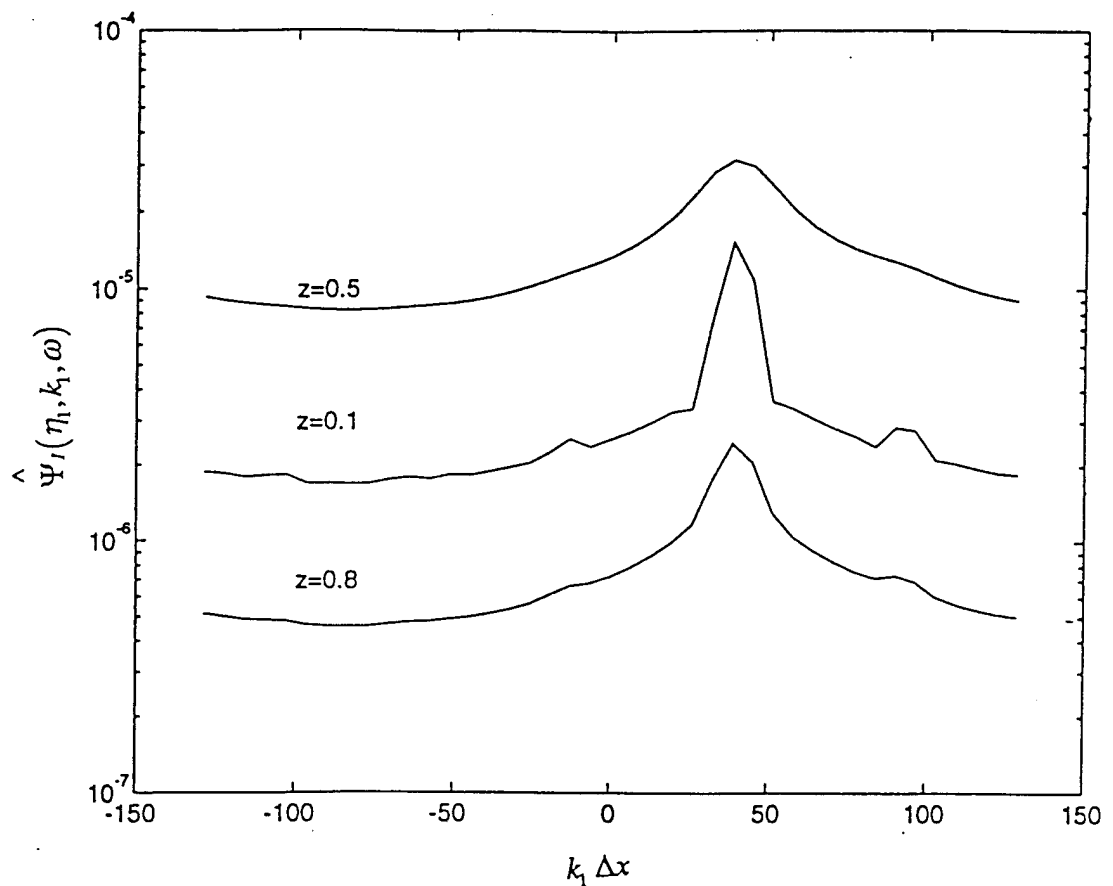


Figure 6. Estimated Space-Dependent Streamwise Wavenumber Spectrum; 50 Hz

and the fact that the mean value could preclude observation of these characteristics, all following estimates of wavenumber spectra presented here will be computed from zero mean estimates of the correlation functions. The second coherent component observed in Figure 6, occurs at a non-dimensional wavenumber of approximately 38. This wavenumber is associated with a phase velocity of 8.23 m/sec suggesting that this is the convective component of the turbulent spots. This component is most visible when $z = 0.1$, and 0.8 . At $z = 0.5$ it is substantially masked by the increased amplitude of the incoherent component. Note that the amplitude of this convective component varies with reference position, and as expected, is therefore non-homogeneous.

The third coherent component is only weakly visible, at a non-dimensional wavenumber of approximately 88, for $z = 0.1$ and 0.8 . This process is completely masked by the incoherent process at $z = 0.5$. It is interesting to note that the phase velocity associated with this wavenumber (3.6 m/sec), is approximately half that of the convective component. The importance of this observation will be developed in a later discussion.

The incoherent process is revealed as the relatively constant amplitude over the wavenumber domain. Note that this process varies with z , so it is therefore non-homogeneous with the greatest amplitude occurring at $z = 0.5$. This is expected because the maximum temporal turbulent spot generation rate occurs in the center of the transition zone¹⁴.

Figure 7 shows the estimated space-varying wavenumber spectra at 100 Hz. Interpretation of these spectra reveal that the same processes that exist at 50 Hz, exist at 100 Hz and are, to some extent, more discernible. The second convective component remains non-homogeneous and occurs at a non-dimensional wavenumber of approximately 76, consistent with the increase in frequency. A third component is seen at a wavenumber of approximately -116. This wavenumber is likely the alias of the actual wavenumber. This hypothesis results from the following considerations. First note that the wavenumber of interest (-116) implies that the direction of propagation is opposite that of the previously identified convective components and therefore not consistent with any expected phenomena. A physically possible phenomena is spatial aliasing. From the previous discussion we know that spatial aliasing will occur at integer multiples of $2\pi/\Delta\epsilon_1$. The estimate of the true wavenumber is determined as $-116 + 2\pi/0.0254 = 131$. This wavenumber suggests a phase speed of 4.8 m/s. Therefore, this wavenumber produces a reasonable interpretation that is consistent with expectations in both wavenumber magnitude and direction of propagation. This phase

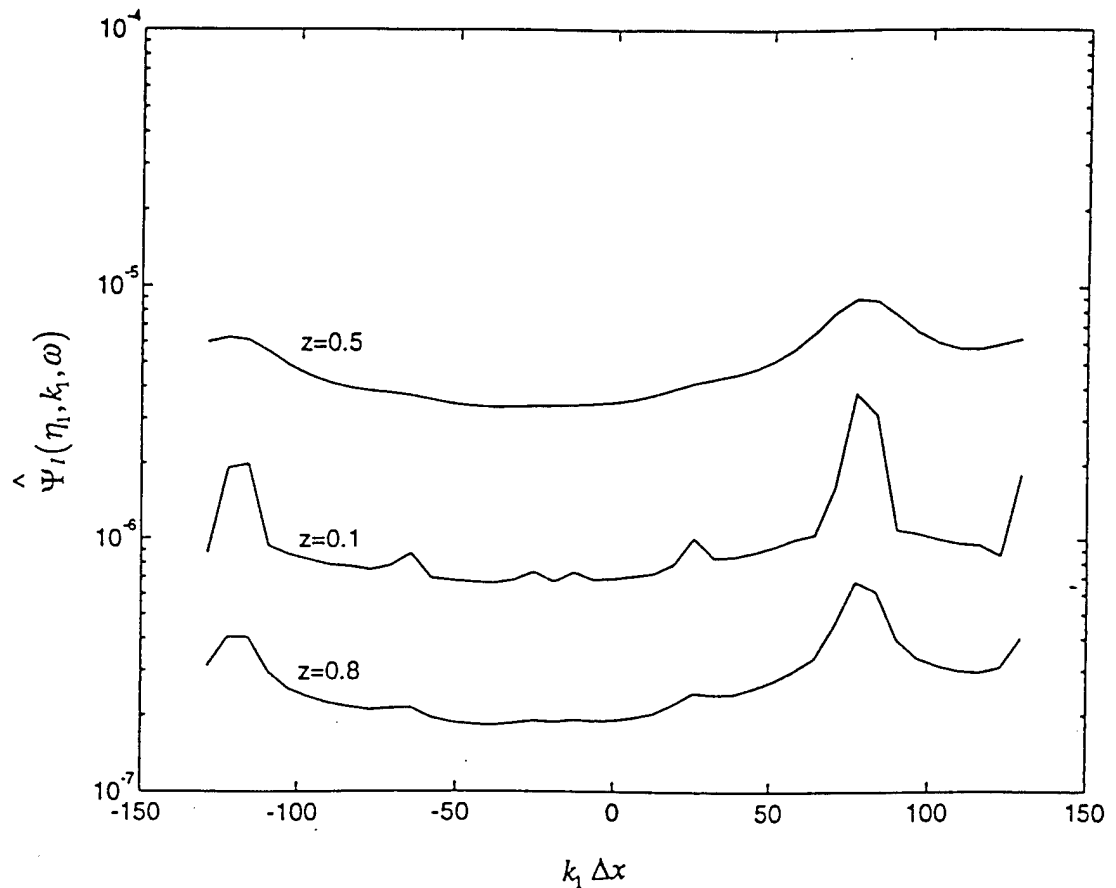


Figure 7. Estimated Space-Dependent Streamwise Wavenumber Spectrum; 100 Hz speed has increased somewhat with frequency but is still approximately half that of the convective component. Specifically, from Figure 6, the phase speed of the third component is $0.31 U_\infty$, while from Figure 7 the phase speed is $0.41 U_\infty$.

Lauchle¹⁴ has reviewed the results of several studies that identify the characteristics of turbulent spot development in a transitioning boundary layer. He notes that turbulent spots typically demonstrate a growth in spatial extent with streamwise propagation. This spatial growth rate implies that the celerity of the leading and trailing evolving turbulent spot edges are different. It is noted that Mautner and Van Atta¹⁵ determine leading and trailing edge pressure convection velocities to be $0.82u_e$ and

$0.55u_e$ where " u_e is the velocity at the outer edge of the laminar boundary layer". This edge velocity is typically $0.99 U_\infty$ for a zero-pressure gradient flat plate flow. From Figure 7 a similar data comparison is $0.7 U_\infty$ and $0.41 U_\infty$ respectively. Although not exact*, these values appear consistent with the reported characteristics. Therefore, it seems reasonable to conjecture that the features observed in the space-varying wavenumber spectra are the result of the turbulent spot generation process. The incoherent process is seen to be non-homogeneous.

Summary of the Space-varying Wavenumber Spectra.

The utility of the space-varying wavenumber spectrum is apparent from only these few examples. The examples, which constitute unprecedented wavenumber-frequency spectral estimates of the transitional flow pressure field, demonstrate that spectral decomposition, in the wavenumber domain, allows separation and identification of processes not obviously apparent in the space-time correlation function. The examples also demonstrate the position dependent nature of non-homogeneous processes. The amplitude of the non-homogeneous components vary with reference location and therefore lack a comprehensive characterization. A more comprehensive characterization is desirable and will be pursued in the following chapter.

* It is noted¹ that the experimental development of an indicator function signal requires the experimenter to set a "threshold" amplitude level of sensor output which identifies turbulent activity. Errors in setting this threshold level would affect the accuracy of spot leading and trailing edge velocities determined from the indicator function signal only.

CHAPTER 3

TWO-WAVENUMBER-FREQUENCY SPECTRUM OF TRANSITION FLOW PRESSURE FIELD

Chapter 2 provides identification and interpretation of transition flow pressure field features using the space-varying wavenumber-frequency spectrum. This spectral format allows immediate classification of dominant pressure field components. However, because the non-homogeneous pressure field spectral amplitude varies with reference position, a composite description of the field cannot be obtained. A solution to this problem is potentially available from a spectral format defined by Strawderman² and denoted the "Two Wavevector-Frequency Spectrum". This spectrum, written in terms of the wavenumber-frequency spectrum of interest to this analysis, is defined as

$$S_{pp}(\mu_1, k_1, \omega) \equiv \int_{-\infty}^{+\infty} \int_{-\infty}^{+\infty} \int_{-\infty}^{+\infty} Q_{pp}(\eta_1, \varepsilon_1, \tau) e^{-i(\mu_1 \eta_1 + k_1 \varepsilon_1 + \omega \tau)} d\eta_1 d\varepsilon_1 d\tau \quad (9)$$

where $Q_{pp}(\eta_1, \varepsilon_1, \tau)$ is the space-time pressure field correlation and μ_1 and k_1 are the Fourier conjugate variables of the absolute spatial vector components η_1 and ε_1 respectively.

Example Two-wavenumber Spectrum

In order to develop a basis for the interpretation of the transition flow pressure, two wavenumber-frequency spectrum, it is useful to construct an example of a non-homogeneous pressure field. The particular example selected is for an exponentially decaying wave and the development parallels that of Strawderman¹⁶.

Let the selected pressure field be defined as

$$p(\eta_l, t) = e^{-\alpha|\eta_l|} \sin(k_0 \eta_l - \omega_0 t + \theta) \quad (10)$$

where η_l is absolute spatial position as before, t is time, α is a positive constant, k_0 and ω_0 are selected wavenumber and radian frequency, and θ is a random variable uniformly distributed in $(-\pi, \pi)$. For $\alpha = 5$, the spatial decay of this field is shown in Figure 8.

Note that the amplitude is substantially reduced over a length consistent with that of the

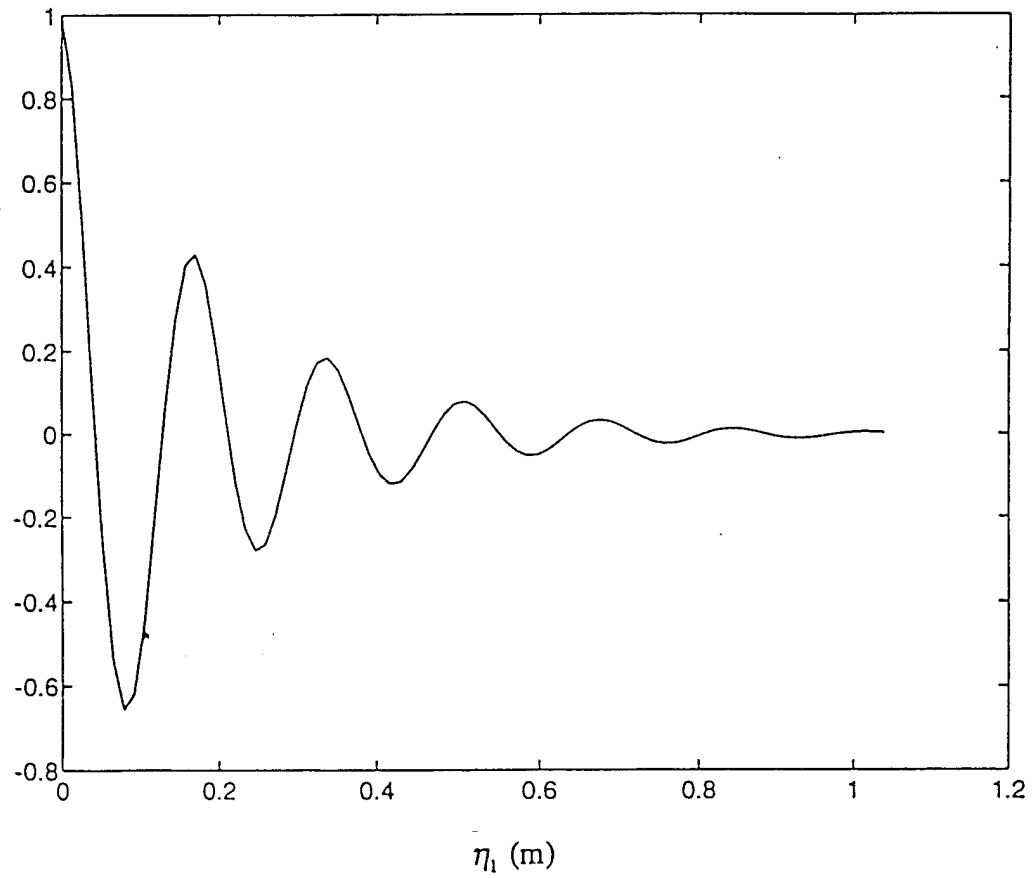


Figure 8. Spatial Decay Characteristics of Example Harmonic Wave

transition zone. The space-time correlation of this pressure field is

$$Q_{pp}(\eta_1, \varepsilon_1, \tau) = \frac{1}{2\pi} \int_{-\pi}^{\pi} e^{-\alpha|\eta_1|} \sin(k_0 \eta_1 - \omega_0 t + \theta) e^{-\alpha|\eta_1 + \varepsilon_1|} \sin(k_0(\eta_1 + \varepsilon_1) - \omega_0(t + \tau) + \theta) d\theta \quad (11)$$

Performing the integration provides the space-time correlation of this non-homogeneous pressure field

$$Q_{pp}(\eta_1, \varepsilon_1, \tau) = \frac{1}{2} e^{-\alpha|\eta_1|} e^{-\alpha|\eta_1 + \varepsilon_1|} \cos(k_0 \varepsilon_1 - \omega_0 \tau) \quad (12)$$

Using (9), the true two wavevector-frequency spectrum is given by

$$S_{pp}(\mu, k, \omega) = 2\pi\alpha^2 \left\{ \frac{\delta(\omega - \omega_0)}{\left[\alpha^2 + (k - k_0)^2 \right] \left[\alpha^2 + (\mu - k + k_0)^2 \right]} + \frac{\delta(\omega + \omega_0)}{\left[\alpha^2 + (k + k_0)^2 \right] \left[\alpha^2 + (\mu - k - k_0)^2 \right]} \right\} \quad (13)$$

From analysis of this functional form Strawderman notes that this two wavevector-frequency spectrum "has relative maxima along the lines $k = k_0$ and $k - \mu = k_0$ and an absolute maximum at the intersection of these lines: that is, at $(\mu, k) = (0, k_0)$ ".

To aid visualization of this characteristic shape it is useful to graphically present the two wavevector-frequency spectrum of (13). Also, to retain focus on transition flow pressure fields, parameters are selected consistent with those of the space-varying wavenumber spectrum computed in Chapter 2. Therefore select $\omega_0 = 306.8$ (rad/s), $k_0 = 37.1$ (rad/m) and $\alpha = 5$ (m⁻¹). A surface plot of (13), using these parameters, is shown in Figure 9.

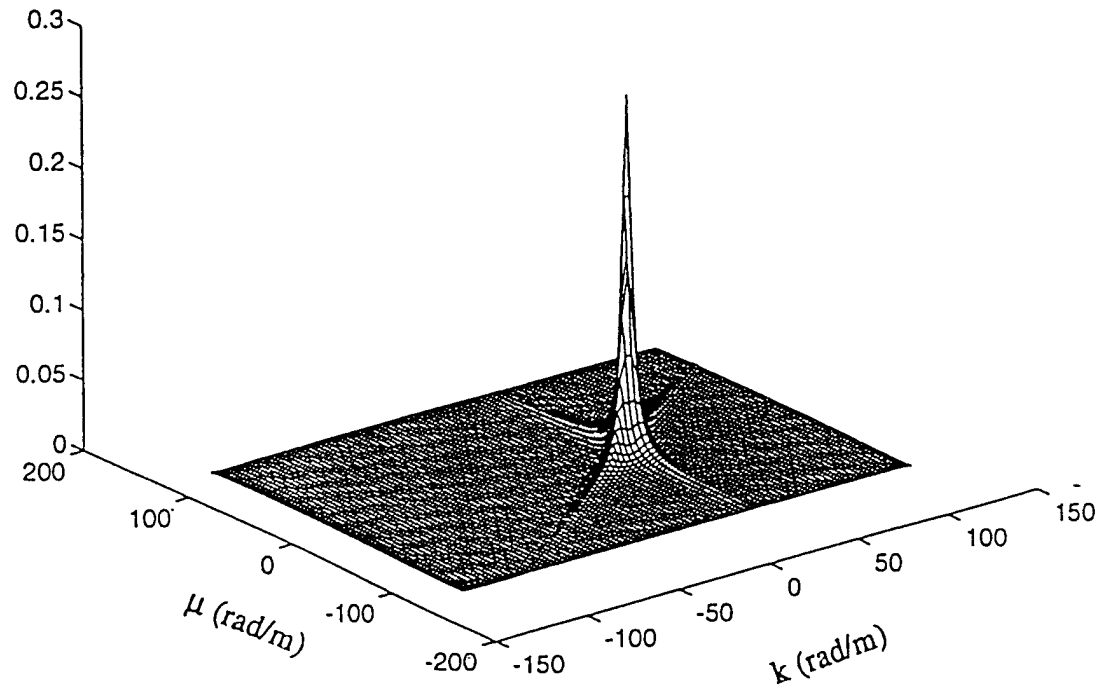
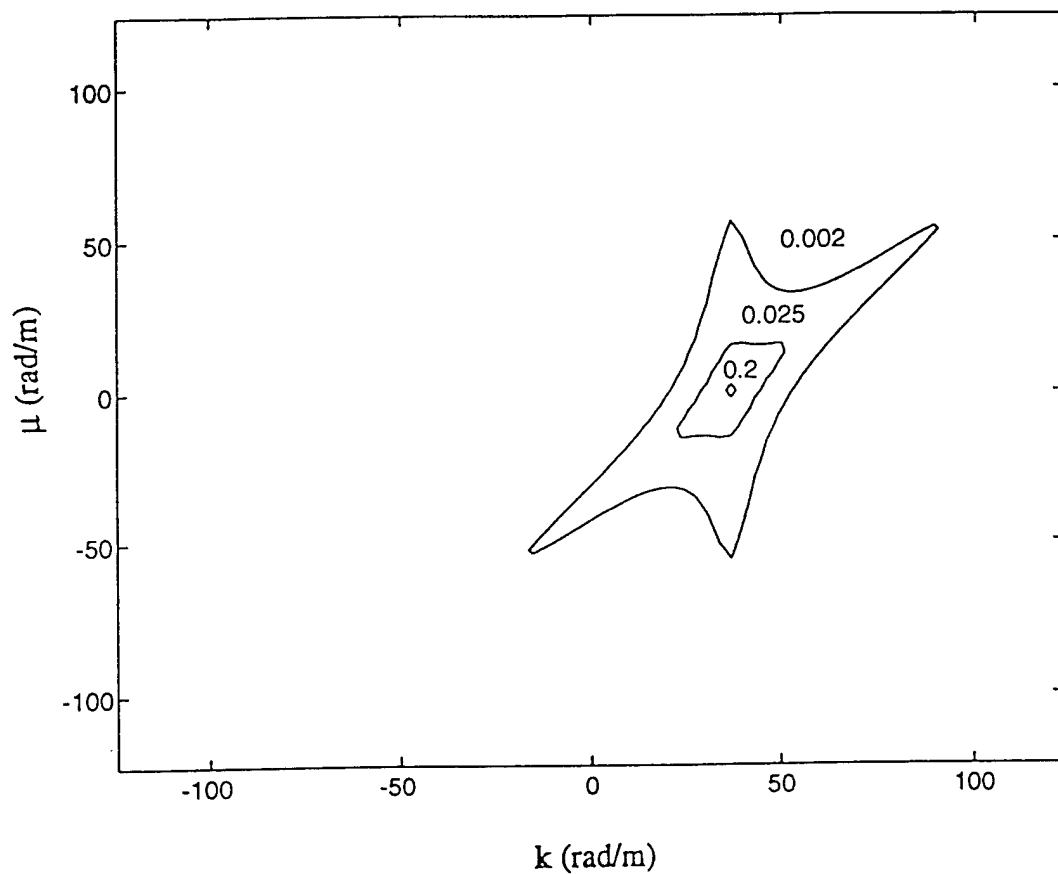


Figure 9. Surface Plot of Exponentially Decaying Single Harmonic Wave True Two-Wavenumber Spectrum

A contour plot of these same values is shown in Figure 10. Note the shape of the contours in the region of the peak value and also that the peak value lies at the intersection of the lines $k_0 = 38.13$ (rad/m) and $k - \mu = k_0$.

Kennedy and Strawderman¹⁷ computed numerical estimates of the two wavenumber-frequency spectrum for an exponentially damped wave. The contour plot of their estimated two wavenumber spectrum is shown in Figure 11. Again note the shape of the contours in the region of the peak value. Kennedy and Strawderman call this shape the "footprint" of an exponentially damped wave.



*Figure 10. Contour Plot of Exponentially Decaying Single Harmonic Wave
Two Wavenumber Spectrum*

A study of the Kennedy and Strawderman work develops intuition for the nature of the two wavenumber spectrum. This allows computation of an estimate for the two wavenumber spectrum of (13) by using the finite Fourier transforms implemented in this research. This is done for both a uniform spatial weighting function and the previously defined Taylor window so that windowing effects can be observed.

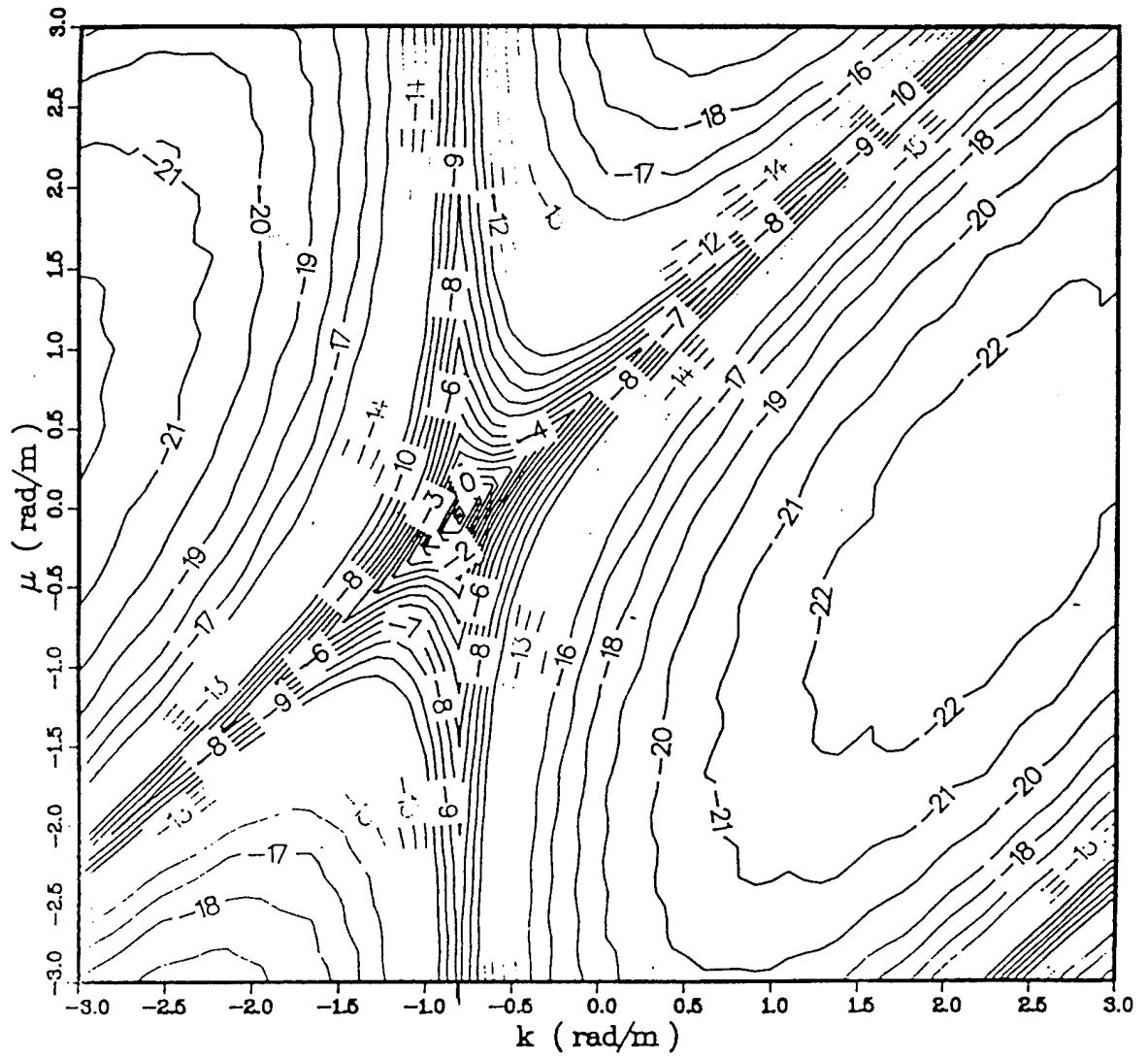


Figure 11. Contour Plot of Two-Wavenumber Spectrum for Unidirectional Exponentially Damped Wave (From Kennedy and Strawderman⁹)

The finite discrete form of (9), required for computer modeling, may be written as

$$\hat{S}_{pp}(\mu_1, k_1, \omega) \propto \sum_{r=1}^R \sum_{n=1}^N \sum_{m=1}^M w_{\eta_1}(r\Delta\eta_1) w_{\epsilon_1}(n\Delta\epsilon_1) w_{\tau}(m\Delta\tau) Q_{pp}(r\Delta\eta_1, n\Delta\epsilon_1, m\Delta\tau) e^{-i(\mu_1 r\Delta\eta_1 + k_1 n\Delta\epsilon_1 - \omega m\Delta\tau)} \Delta\eta_1 \Delta\epsilon_1 \Delta\tau \quad (14)$$

where $\hat{S}_{pp}(\mu_1, k_1, \omega)$ identifies the two-wavenumber spectral estimate, and $w_{\eta_1}(r\Delta\eta_1)$ is an additional spatial weighting function. All other variables are as previously defined. For the first calculation the spatial weights are set to unity. A two-wavenumber spectral estimate surface plot of the damped harmonic wave is shown in Figure 12.

A contour plot of the same estimate is shown in Figure 13. Note that the expected "footprint" is indeed obtained.

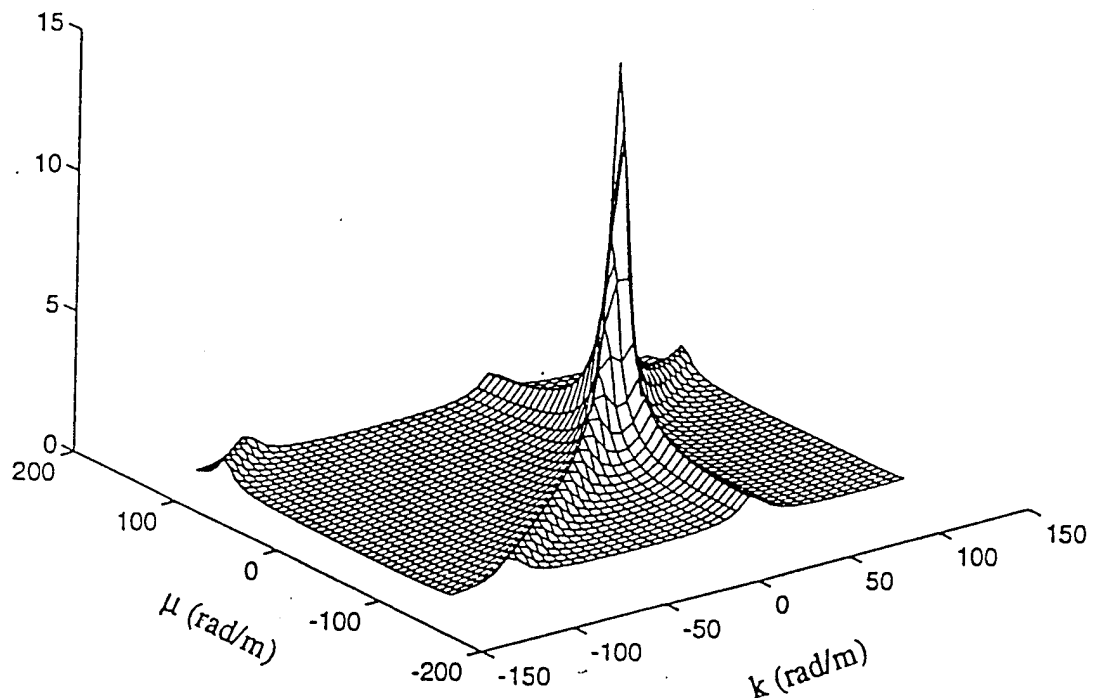


Figure 12. Surface Plot of Estimated Two-Wavenumber Spectrum of Example Exponentially Decaying Single Harmonic Wave Using Unit Spatial Weighting

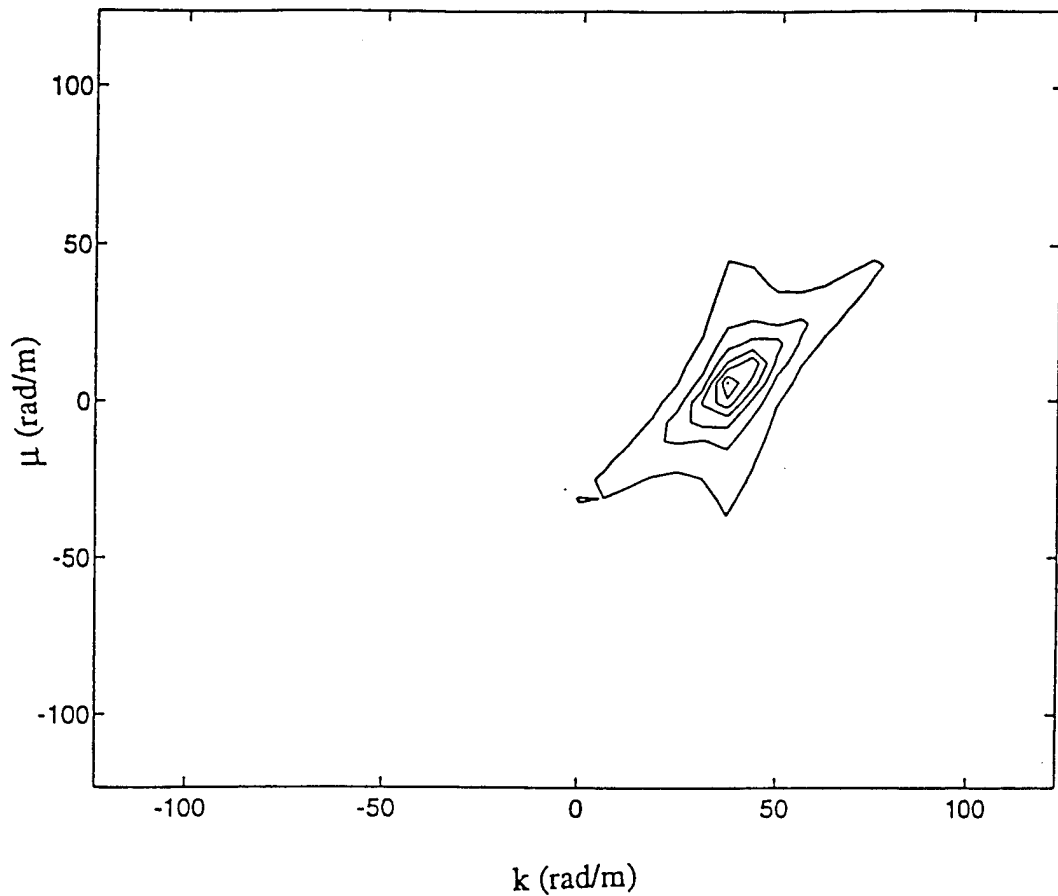


Figure 13. Contour Plot of Estimated Two-Wavenumber Spectrum of Example Exponentially Decaying Single Harmonic Wave Using Unit Spatial Weighting

Since, in general, weighting functions are required to compute numerical spectral estimates it is appropriate to now apply them to this idealized waveform. This is implemented by replacing the previously applied uniform weights with Taylor weights and repeating the calculation. A surface plot of the two-wavenumber spectral estimate using Taylor weights is shown in Figure 14.

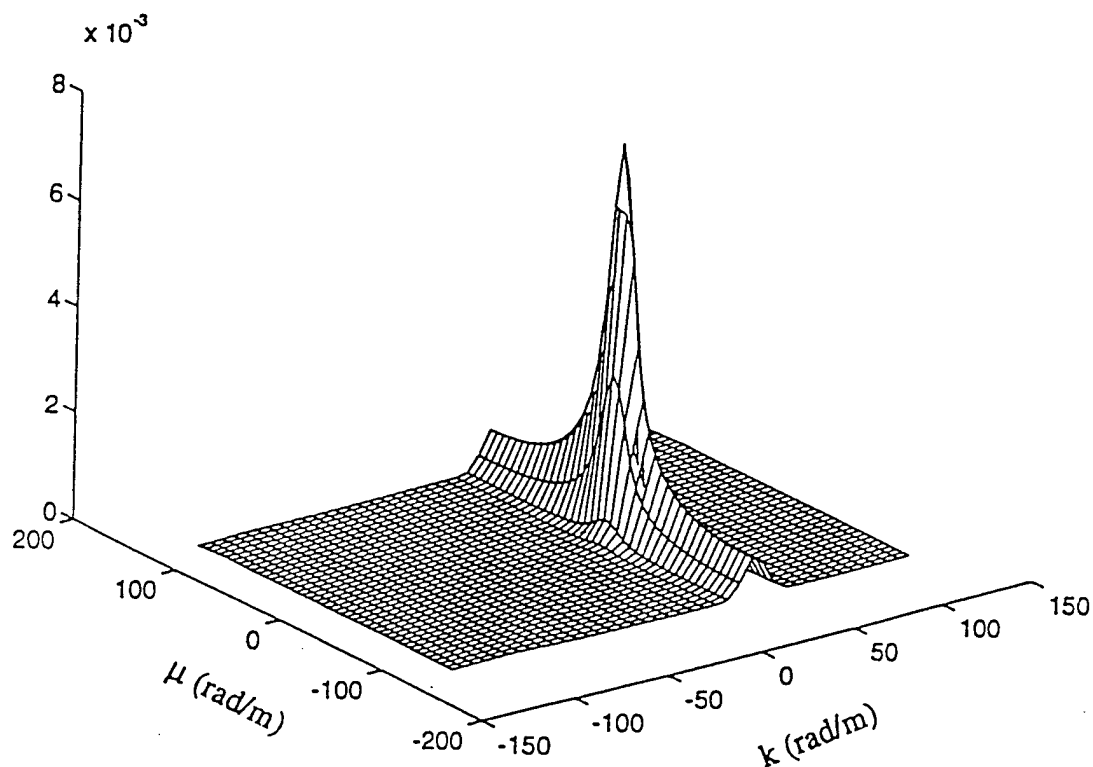


Figure 14. Surface Plot of Estimated Two-Wavenumber Spectrum of Example Exponentially Decaying Single Harmonic Wave Using Taylor Spatial Weighting

A contour plot of the same estimate is shown in Figure 15. Note that the effect of the weighting functions is to broaden the response in the region of the peak and reduce amplitudes in regions removed from the peak. This is entirely consistent with the previous discussion regarding the trade-off between main lobe width and sidelobe level. For this single component example, the selected window appears to be poor choice. However, it must be remembered that the window was selected to reduce sidelobe level leakage so that low level components might be identified. The utility of this window was demonstrated in Figure 6, where the low level trailing edge component velocities were

observed. It is likely that these low level components would not have been visible if a window with less sidelobe rejection was used. It is believed that this window remains an appropriate choice for the spectral estimates of interest in this research.

This example provides a basis for the interpretation of the two-wavenumber spectrum of a single, exponentially decaying wave. It is observed that this two-wavenumber spectrum has a characteristic shape in the μ, k spectrum that contains an absolute peak at $(\mu, k) = (0, k_0)$ and relative maxima along the line $k - \mu = k_0$.

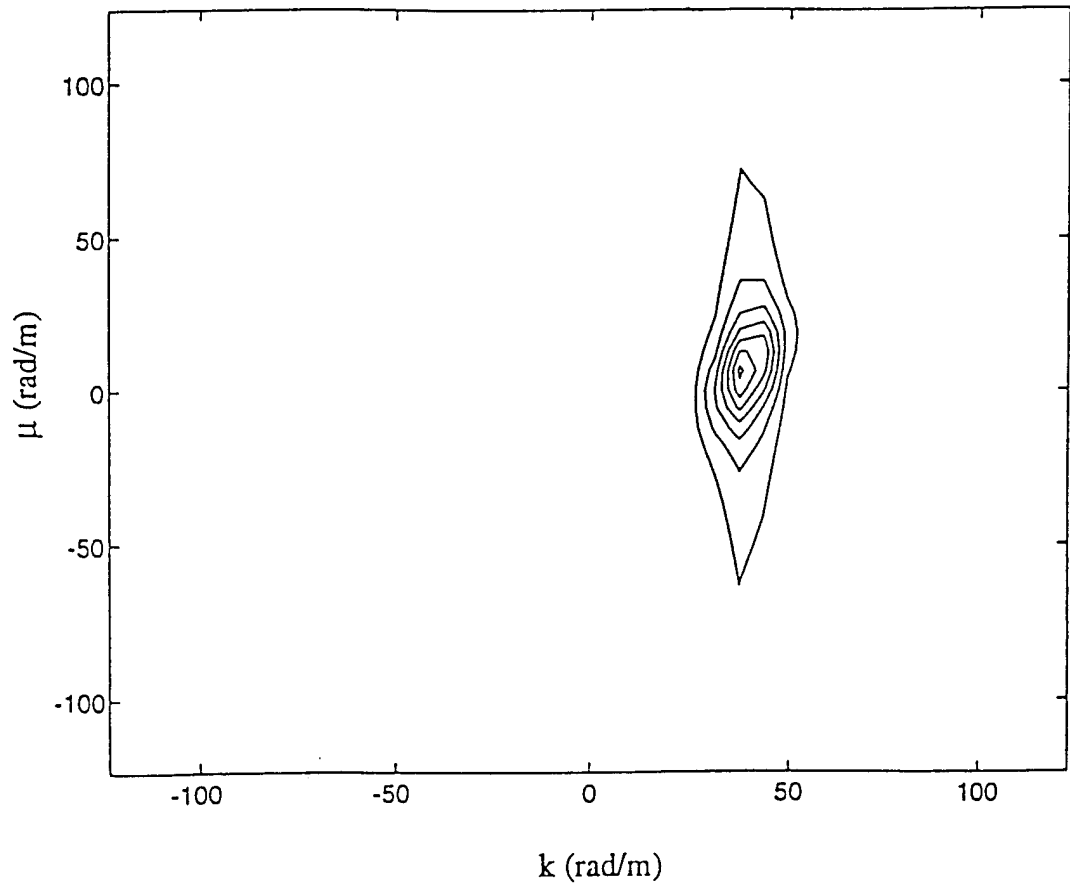


Figure 15. Contour Plot of Estimated Two-Wavenumber Spectrum of Example Exponentially Decaying Single Harmonic Wave Using Taylor Spatial Weighting

Two-Wavenumber Transitional Flow Pressure Field Spectrum

An estimate of the streamwise transitional flow pressure field two wavevector-frequency spectrum is implemented by substituting $R_I(\eta_1, \varepsilon_1, 0, \tau)$ into (14) yielding

$$\hat{S}_{pp}(\mu_1, k_1, \omega) \propto \sum_{r=1}^R \sum_{n=1}^N \sum_{m=1}^M w_{\eta_1}(r\Delta\eta_1) w_{\varepsilon_1}(n\Delta\varepsilon_1) w_{\tau}(m\Delta\tau) R_I(r\Delta\eta_1, n\Delta\varepsilon_1, 0, m\Delta\tau) e^{-i(\mu_1 r\Delta\eta_1 + k_1 n\Delta\varepsilon_1 - \omega m\Delta\tau)} \Delta\eta_1 \Delta\varepsilon_1 \Delta\tau \quad (15)$$

where $R_I(\eta_1, \varepsilon_1, 0, \tau)$ is the previously defined space-time correlation of the intermittency indicator function, and μ_1 and k_1 are now the Fourier conjugate variables of η_1 and ε_1 respectively.

The surface plot of the 50 Hz two-wavenumber spectrum is shown in Figure 16. The contour plot of the same spectrum is shown in Figure 17. These spectra were calculated using the Taylor temporal and spatial weights. Three observations may be made: 1) the absolute spectral peak occurs at $\mu = 0$ and the convective wavenumber ($k_0 = 37.1$), 2) the line $k - \mu = k_0$, is perceptible only in the region of the peak, 3) relative maxima occur at all k -wavenumbers at $\mu = 0$. The location of the absolute peak is as expected and needs no further discussion. However, the other two observations warrant further consideration.

Recall, from the exponentially decaying wave example, that the effect of the application of spatial weighting was to obscure the visualization of the relative maxima line ($k - \mu = k_0$). This is likely the result of the wider main lobe and lower sidelobes of the spatial window. Also, recall that the example was for a single wave at an arbitrary

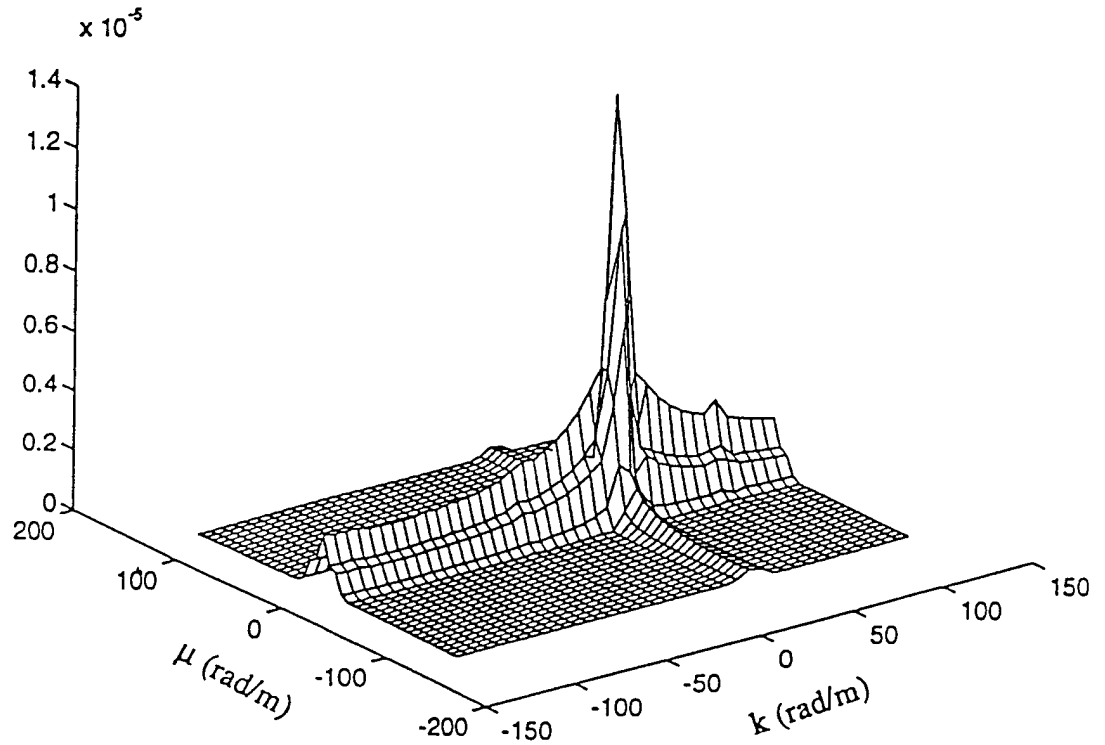


*Figure 16. Surface Plot of Estimated Streamwise Transitional Flow Pressure Field
Two-Wavenumber Spectrum at 50 Hz*

wavenumber k_0 . It is to be expected that another independent wave, at a different k -wavenumber, would create a similar shape but the footprint would be displaced somewhere else consistent with the selected wavenumber. Now assume that the transitional flow pressure field is the superposition of a continuous distribution of such components. With this assumption the wavenumber spectra at $\mu = 0$ would represent the propagating wavenumber spectrum of the transition flow pressure field. Furthermore, the spectral contributions of any given component along the line $k - \mu = k_0$ would merge with

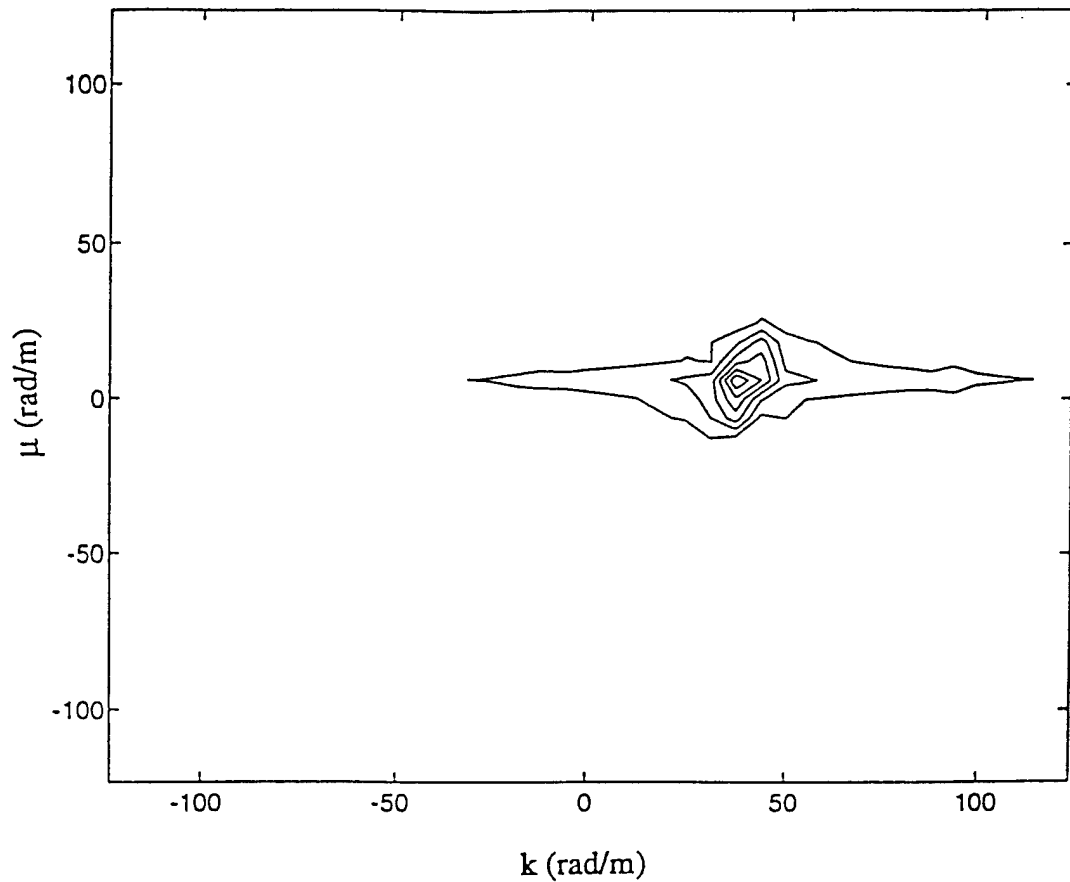


*Figure 17. Contour Plot of Estimated Streamwise Transition Flow Pressure Field
Two-Wavenumber Spectrum at 50 Hz*

those of adjacent spectral components, destroying the characteristic "footprint" observed in the example. With these considerations it is believed that Figures 16 and 17 are valid representations of the two-wavenumber spectrum of the transitional flow pressure field.

To complete this presentation the two-wavenumber spectrum at 100 Hz is calculated. The surface plot of this spectrum is shown in Figure 18.

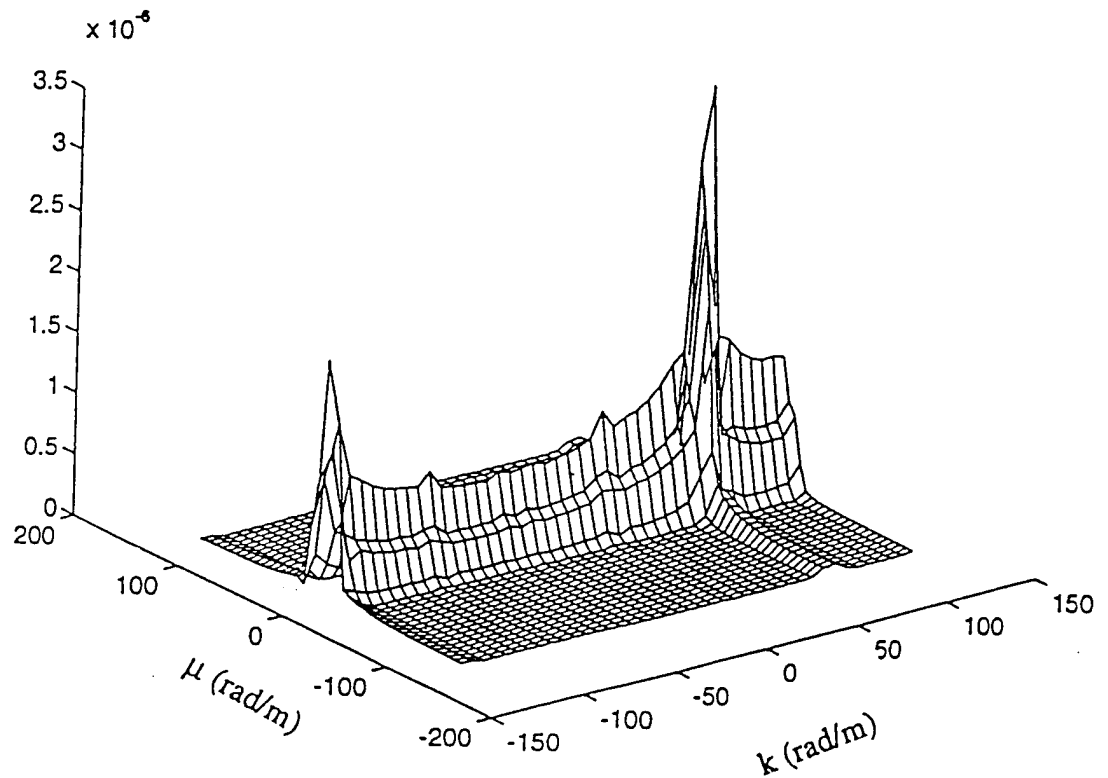


*Figure 18. Surface Plot of Estimated Streamwise Transition Flow Pressure Field
Two-Wavenumber Spectrum at 100 Hz*

The contour plot is shown in Figure 19. Note that the absolute peak value is again at the convective wavenumber. Also note that a lower but significant peak occurs at a k wavenumber of approximately -116. This is consistent with the turbulent spot generation process noted in the space-varying spectrum. It is apparent then that the two-wavenumber spectrum provides the same information available from the multiple space-varying wavenumber spectra, but in a single concise format.

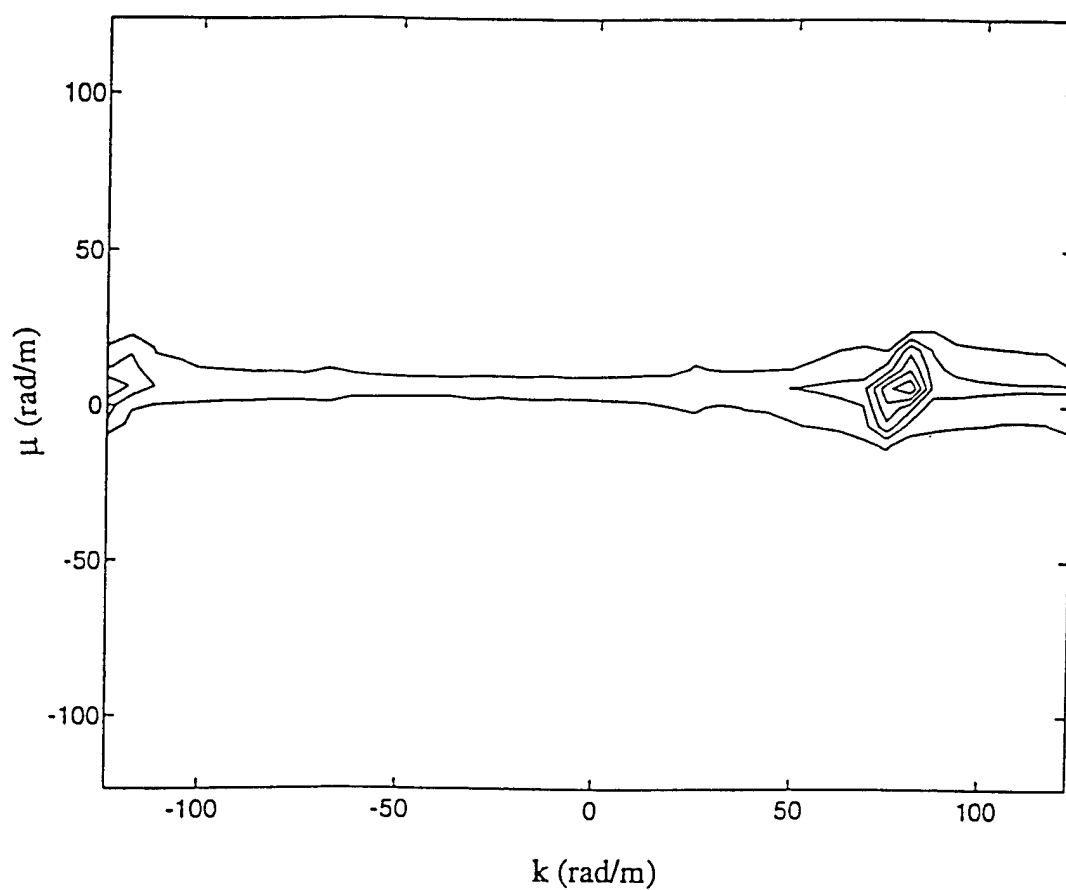


*Figure 19. Contour Plot of Estimated Streamwise Transition Flow Pressure Field
Two-Wavenumber Spectrum at 100 Hz*

Summary of the Two-Wavenumber Spectra.

A two-wavenumber spectrum has been defined that provides a concise description of non-homogeneous fields. The characteristics of this two-wavenumber spectrum have been identified using a non-homogeneous pressure field example containing parameters pertinent to a subsonic boundary layer transition zone. Transition zone flow pressure field estimates for the two-wavenumber spectrum have been computed at two frequencies of interest. These two-wavenumber spectral estimates provide a full spectral, concise form of the information contained in the associated multiple space-varying wavenumber-frequency spectra. The results of this research demonstrate that the two-wavenumber spectrum provides a concise, full spectral representation of the streamwise transitional flow pressure field.

CHAPTER 4

CONCLUSIONS AND RECOMMENDATIONS

This research has implemented a computer model to produce unprecedented images of the non-homogeneous, transitional flow pressure field wavenumber-frequency spectrum, in two formats. The first format, called the space-varying wavenumber-frequency spectrum, accommodates non-homogeneous fields by presenting the familiar wavenumber-frequency spectrum in terms of an absolute spatial reference position parameter. Because the field is non-homogeneous, multiple wavenumber spectra must be computed to display the field characteristics. This research provides these multiple wavenumber spectra at two frequencies of interest. Analysis of these space-varying wavenumber-frequency spectral estimates suggest that more than one convective component exists in the transition zone indicator function.

There is a consistently prominent convection wavenumber $k_0 = \omega_0 / U_c$, where U_c is the average convection speed of the turbulent spots. And, there also appears a higher wavenumber component corresponding to a much lower convection speed than the average convection speed. The speeds computed from the spectral information suggest that these lower convection speeds are associated with the much slower trailing edge velocity of the turbulent spots within the transition zone. This identification would not have been possible from a study of the space-time correlation functions alone. This demonstrates the power of the wavenumber spectral representation in uncovering important physical features of complex non-homogeneous fields.

The second wavenumber-frequency spectral format is newly defined and called the two-wavenumber-frequency spectrum. This format is an extension of the space-varying wavenumber-frequency spectrum and provides a full spectral representation of a non-homogeneous field. This format has the distinct advantage of providing a concise presentation of the wavenumber spectral properties of the field, at a given frequency, in a single image. Associated with the advantages of conciseness is the need to develop knowledge and intuition with the new and somewhat unfamiliar μ wavenumber domain.

It is recommended that this knowledge be pursued and that this spectral technique be utilized in future experimental efforts involving non-homogeneous random fields. It would be particularly valuable in transition zone wall pressure fluctuation studies to provide direct measurement of the pressure field. With the entire pressure signal available, it is believed that the two-wavenumber spectral representation would yield accurate estimates of the leading and trailing edge spot convection velocities as well as the average spot convection velocity. Remember that the indicator function used here was for natural turbulent spots that are created at random in both space and time. The work of Ref [15], which identified leading and trailing edge celerities, used single spots created deterministically. Here, we have uncovered almost the same information for randomly occurring spots in a naturally occurring transition zone.

REFERENCES

1. M. A. Josserand and G. C. Lauchle, "Modeling the Wavevector-Frequency Spectrum of Boundary Layer Wall Pressure During Transition on a Flat Plate," *Journal of Vibration and Acoustic*, Vol 112, October 1990.
2. W. A. Strawderman, "Wavevector-Frequency Spectra Of Nonhomogeneous Fields", NUSC Technical Document 7873, Naval Underwater Systems Center, New London, CT, 22 January 1987.
3. M. A. Josserand and G. C. Lauchle, "Wavevector-Frequency Spectrum of Transition Zone Wall Pressure Fluctuations," Applied Research Laboratory, Technical Report TR 86-008, p 81, The Pennsylvania State University, State College, PA , December 1986.
4. W. A. Strawderman, *Wavevector-Frequency Analysis with Applications to Acoustics*, p 9-5, U. S. Government Printing Office, Washington, DC 20402
5. *ibid*, p 8-20/8-32
6. F. J. Harris, "On the Use of Windows for Harmonic Analysis with the Discrete Fourier Transform," p 53 & 54 *Proceedings of the IEEE*, Vol. 66, No. 1, January 1978
7. *ibid*, p 52 & 53

8. W. A. Strawderman, *Wavevector-Frequency Analysis with Applications to Acoustics*, p 8-2, U. S. Government Printing Office, Washington, DC 20402
9. M. A. Josserand and G. C. Lauchle, "Wavevector-Frequency Spectrum of Transition Zone Wall Pressure Fluctuations," Applied Research Laboratory, Technical Report TR 86-008, p 27, The Pennsylvania State University, State College, PA , December 1986.
10. J. S. Bendat and A. G. Piersol, *Random Data Analysis and Measurement Procedures*, 2nd Edition, p335, John Wiley & Sons, New York, 1986
11. W. A. Strawderman, *Wavevector-Frequency Analysis with Applications to Acoustics*, p 8-38, U. S. Government Printing Office, Washington, DC 20402
12. *ibid*, p 8-35
13. R. L. Streit, "A Discussion of Taylor Weighting for Continuous Apertures," NUSC Technical Memorandum 851004, Naval Underwater Systems Center, New London, CT, 4 January 1985.
14. G. C. Lauchle, "Hydroacoustics Of Transitional Boundary-Layer Flow," *Appl Mech Rev*, Vol 44, no 12, part 1, December 1991.
15. T. S. Mautner and C. W. Van Atta, "An Experimental Study of the Wall-Pressure Field Associated with a Turbulent Spot in a Laminar Boundary Layer," *J. Fluid Mech* 118, 59 (1982)

INITIAL DISTRIBUTION LIST

Addressee	No. of Copies
Defense Technical Information Center	12
Program Executive Office-USW-ASTO-D3 (C. Traweek)	1
Office of Naval Research (V. Simmons (ONR-334), R. Varley (ONR-321), S. Littlefield (ONR-321))	3
Pennsylvania State University (G. Lauchle)	1
BBN, Cambridge (N. Martin, G. Duckworth)	2
BBN, New London (J. Webster)	1
Cambridge Acoustical Associates (J. Garrellick, J. Cole)	2
H. P. Bakewell, Old Saybrook, CT	1
W. A. Strawderman, Ledyard, CT	1